Experimental Evidence for a Dynamical Non-Locality Induced Effect in Quantum Interference Using Weak Values

S. E. Spence and A. D. Parks

Quantum Processing Group, Electromagnetic and Sensor Systems Department,

Naval Surface Warfare Center, Dahlgren, VA 22448 USA

(Dated: Experimental / Draft Completion.....January 19, / March 12, 2010)

Abstract

The quantum theoretical concepts of modular momentum and dynamical non-locality, which were introduced four decades ago, have recently been used to explain single particle quantum interference phenomena. Although the non-local exchange of modular momentum associated with such phenomena cannot be directly observed, it has been suggested that effects induced by this exchange can be measured experimentally using weak measurements of pre- and post-selected ensembles of particles. This paper reports on such an optical experiment that yielded measured weak values that were consistent with the theoretical prediction of an effect induced by a non-local exchange of modular momentum.

I. INTRODUCTION

Because it differs fundamentally from the interference phenomena of classical physics, quantum interference has remained a continuing topic for discussion and debate since quantum theory's early days. The essence of this difference is exhibited by the two-slit experiment. From both the classical and Schrödinger wave perspectives, the two slit interference pattern is easily described in terms of the overlapping contributions of the wave which have passed through each slit. The wave perspective also explains the disappearance of the interference pattern when one of the slits is closed.

However, interference experiments using low intensity electron or photon beams in which only one particle at a time passes through a two-slit apparatus have shown that the accumulated effect when both slits are open is an interference pattern like that produced by higher intensity ensembles and that the pattern likewise disappears when one slit is closed, e.g. [1]. This peculiar behavior necessitates an answer to the question "how does a particle passing through one slit sense that the other slit is open or closed?" when interference is considered from the perspective of a single quantum particle.

Although this question concerning single particle behaviour has been answered and explained theoretically in terms of a non-local exchange of modular momentum [2, 3], there have been no direct experimental observations of such an exchange to support this explanation. This lack of observations is due to the fact that the conditions required to observe a non-local exchange of modular momentum are precisely those that make the associated modular variable completely uncertain and unobservable. Recently, however, it was suggested that an experimental methodology using weak measurements performed on a pre- and post-selected ensemble of particles could be exploited in order to observe an effect *induced* by a non-local exchange of modular momentum. This methodology was illustrated by a *gedanken* experiment which used a twin Mach-Zehnder interferometer to duplicate relevant aspects of the two-slit interference experiment [4].

This paper reports the results of an optical twin Mach-Zehnder interferometer experiment similar to that described in the above *gedanken* experiment. This experiment yielded measured weak values that were consistent with the associated theoretical prediction describing the effect induced by a non-local exchange of modular momentum. The remainder of this paper is organized as follows: in the next section the theories of modular momentum,

dynamical non-locality, weak measurements, and weak values are briefly summarized. A description of the experimental apparatus and an overview of the experiment are presented in section III. The experimental results are discussed in section IV. Concluding remarks comprise the final section of this paper.

II. SUMMARY OF THE THEORIES

A. Modular Momentum and Dynamical Non-locality

Consider a quantum particle propagating in the positive y-direction perpendicular to the plane of two symmetric slits which are separated by a distance ℓ in the x-direction (the slit at $x-\ell$ will be referred to as the left slit). At time t after the particle passes through the slits its wavefunction is the superposition

$$\psi(x,y,z,t)=\frac{1}{\sqrt{2}}\left\{\varphi(x-\ell,y,z,t)+e^{i\alpha}\varphi(x,y,z,t)\right\}, \tag{1}$$

where the φ's are assumed to be identical "wave packets" which do not overlap at $t=0$ and α is their relative phase. Although information about α can be obtained from the spatial interference pattern $|\psi(x,d,z,\tau)|^2$ produced by an ensemble of such particles on a screen parallel to and at an appropriate distance d from the plane of the slits at time $\tau>0$, there are no local measurements using operators of the form $\widehat{x}^j\widehat{p}_x^k$, where j and k are non-negative integers, that can be performed upon the initial non-overlapping wave packets that will determine α. The relative phase α is thus a non-local feature of quantum mechanics.

The induced momentum uncertainty and the Heisenberg uncertainty principle are traditionally used to explain the loss of the interference pattern when one slit is closed. However, measuring which slit the particle passes through does not necessarily increase the momentum uncertainty. This - along with the fact that position and momentum observables and their moments are not sensitive to relative phase (prior to wave packet overlap) - suggests that these observables, as well as the Heisenberg uncertainty principle, are not the appropriate physical concepts for describing quantum interference phenomena.

The (modular) operator $e^{-\frac{i}{\hbar}\widehat{p}_x\ell}$ and its modular property, however, do provide an alternative physical basis for the rational description of quantum interference. Unlike the operators $\widehat{x}^j\widehat{p}_x^k$, the expectation value of the operator $e^{-\frac{i}{\hbar}\widehat{p}_x\ell}$ with respect to $\psi(x,y,z,t)$ is sensitive to α - even when the two wavepackets don't overlap. This sensitivity results

from the action of $e^{-\frac{i}{\hbar}\widehat{p}_x\ell}$ upon $\varphi(x,y,z,t)$ which overlaps the two wavepackets in eq. (1) by translating $\varphi(x,y,z,t)$ to $\varphi(x-\ell,y,z,t)$. Also, since $e^{-\frac{i}{\hbar}\widehat{p}_x\ell}$ is invariant under the replacement $\widehat{p}_x \to \widehat{p}_x - n\frac{h}{\ell}$, $n = 0, \pm1, \pm2, \cdots$, (because $e^{-\frac{i}{\hbar}(-n\frac{h}{\ell})\ell} = e^{2in\pi} = 1$), it depends upon values of the *modular momentum* $p_x \bmod \left(\frac{nh}{\ell}\right) \equiv p_{x,\mathrm{mod}} \in I \equiv [0, \frac{h}{\ell})$ instead of those of p_x. This modular property establishes a fundamental relationship between modular momentum uncertainty and quantum interference via the complete uncertainty principle: "$\widehat{p}_{x,\mathrm{mod}}$ is completely uncertain (i.e. all its values are uniformly distributed over I) if and only if $\left\langle e^{-\frac{i}{\hbar}n\widehat{p}_x\frac{\ell}{\hbar}} \right\rangle = 0$ for every positive integer n". When this principle is applied to the two slit case, it is found that while the required expectation value with respect to $\psi(x,y,z,t)$ does not vanish for $n = 1$, it does vanish for every n when the expectation value is with respect to $\varphi(x,y,z,t)$. Thus, when the left slit is closed, i.e. it is known that the particle passed through the right slit, then $\widehat{p}_{x,\mathrm{mod}}$ becomes completely uncertain so that all knowledge about $p_{x,\mathrm{mod}}$ is lost and the interference pattern vanishes.

The Heisenberg equation of motion provides the formalism for describing and understanding the notion of *dynamical non-locality*. Within the context of two slits, the Heisenberg equation of motion for $e^{-\frac{i}{\hbar}\widehat{p}_x\ell}$ is given by

$$\frac{d}{dt}e^{-\frac{i}{\hbar}\widehat{p}_x\ell} = \frac{i}{\hbar}\left[\widehat{H}, e^{-\frac{i}{\hbar}\widehat{p}_x\ell}\right] = \frac{i}{\hbar}\left(\widehat{V}(x) - \widehat{V}(x-\ell)\right)e^{-\frac{i}{\hbar}\widehat{p}_x\ell}, \tag{2}$$

where $\widehat{H} = \frac{\widehat{p}_x^2}{2m} + \widehat{V}(x)$ is the system Hamiltonian and $\widehat{V}(x)$ ($\widehat{V}(x-\ell)$) is the potential operator for the right (left) slit. This is a non-local equation of motion and therefore has no classical analogue: only the potential at each slit is involved in the rate of change of $e^{-\frac{i}{\hbar}\widehat{p}_x\ell}$ - i.e. there are no forces involved - and the potential at the left slit influences this rate of change even if $\psi(x,y,z,0) = \varphi(x,y,z,0)$ - i.e. when the particle is initially localized at the right slit. Consequently, the effect of closing the left slit produces non-locally a change in modular momentum while leaving the expectation values of the associated moments of momentum unchanged. More specifically, the modular operator is conserved when both slits are open since $\widehat{V}(x) = \widehat{V}(x-\ell)$ so that $\frac{d}{dt}e^{-\frac{i}{\hbar}\widehat{p}_x\ell} = 0$. However, if the left slit is closed and the particle is localized at the right slit, then $\left(\widehat{V}(x) - \widehat{V}(x-\ell)\right) \neq 0 \neq \frac{d}{dt}e^{-\frac{i}{\hbar}\widehat{p}_x\ell}$ and the modular momentum is changed non-locally as a result of the change in the potential at the left slit. Interference is destroyed and the modular momentum becomes completely uncertain - thereby rendering it unobservable. In fact, it is in this manner that the complete uncertainty principle also reconciles dynamical non-locality with causality.

For additional details concerning the theory of modular momentum and dynamical non-locality the reader is invited to consult references [2–5].

B. Weak Measurements and Weak Values

Although the exchange of modular momentum is not directly observable, it has been suggested that dynamical non-locality induces effects which can be observed using weak measurements of pre- and post-selected ensembles of particles. Weak measurements arise in the von Neumann description of a quantum measurement at time t_0 of a time-independent observable $\widehat{A}$ that describes a quantum system in an initial fixed pre-selected state $|\psi_i\rangle = \sum_J c_j |a_j\rangle$ at t_0, where the set J indexes the eigenstates $|a_j\rangle$ of $\widehat{A}$. In this description the Hamiltonian for the interaction between the measurement apparatus and the quantum system is

$$\widehat{H} = \gamma(t)\widehat{A}\widehat{p}.$$

Here $\gamma(t) = \gamma\delta(t - t_0)$ defines the strength of the impulsive measurement interaction at t_0 and $\widehat{p}$ is the momentum operator for the pointer of the measurement apparatus which is in the initial state $|\phi\rangle$. Let $\widehat{q}$ be the pointer's position operator that is conjugate to $\widehat{p}$ and assume that $\langle q|\,\phi\rangle \equiv \phi(q)$ is real valued with $\langle q\rangle \equiv \langle\phi|\,\widehat{q}\,|\phi\rangle = 0$.

Prior to the measurement the pre-selected system and the pointer are in the tensor product state $|\psi_i\rangle\,|\phi\rangle$. Immediately following the measurement the combined system is in the state

$$|\Phi\rangle = e^{-\frac{i}{\hbar}\int \widehat{H}dt}\,|\psi_i\rangle\,|\phi\rangle = \sum\nolimits_J c_j e^{-\frac{i}{\hbar}\gamma a_j \widehat{p}}\,|a_j\rangle\,|\phi\rangle\,,$$

where use has been made of the fact that $\int \widehat{H}dt = \gamma\widehat{A}\widehat{p}$. The exponential factor in this equation is the translation operator $\widehat{S}(\gamma a_j)$ for $|\phi\rangle$ in its q-representation. It is defined by the action $\langle q|\,\widehat{S}(\gamma a_j)\,|\phi\rangle = \langle q - \gamma a_j|\,\phi\rangle \equiv \phi(q - \gamma a_j)$ which translates the pointer's wavefunction over a distance γa_j parallel to the q-axis. The q-representation of the combined system and pointer state is

$$\langle q|\,\Phi\rangle = \sum\nolimits_J c_j\,\langle q|\,\widehat{S}(\gamma a_j)\,|\phi\rangle\,|a_j\rangle\,.$$

When the measurement interaction is strong, the quantum system is appreciably disturbed and its state "collapses" to an eigenstate $|a_n\rangle$ leaving the pointer in the state $\langle q|\,\widehat{S}(\gamma a_n)\,|\phi\rangle$ with probability $|c_n|^2$. Strong measurements of an ensemble of identically

prepared systems yield $\gamma \langle A \rangle \equiv \gamma \langle \psi_i | \widehat{A} | \psi_i \rangle$ as the centroid of the pointer probability distribution

$$|\langle q| \Phi \rangle|^2 = \sum\nolimits_J |c_j|^2 \left| \langle q| \widehat{S}(\gamma a_j) |\phi\rangle \right|^2 \tag{3}$$

with $\langle A \rangle$ as the measured value of $\widehat{A}$.

A *weak measurement* of $\widehat{A}$ occurs when the interaction strength γ is sufficiently small so that the system is essentially undisturbed and the uncertainty Δq is much larger than $\widehat{A}$'s eigenvalue separation. In this case, eq.(3) is the superposition of broad overlapping $\left| \langle q| \widehat{S}(\gamma a_j) |\phi\rangle \right|^2$ terms. Although a single measurement provides little information about $\widehat{A}$, many repetitions allow the centroid of eq.(3) to be determined to any desired accuracy.

If a system state is post-selected after a weak measurement is performed, then the resulting pointer state is

$$|\Psi\rangle = \langle \psi_f | \Phi \rangle = \sum\nolimits_J c_j'^* c_j \widehat{S}(\gamma a_j) |\phi\rangle ,$$

where $|\psi_f\rangle = \sum_J c_j' |a_j\rangle$, $\langle \psi_f | \psi_i \rangle \neq 0$, is the post-selected state at t_0. Since

$$\widehat{S}(\gamma a_j) = \sum_{m=0}^{\infty} \frac{[-i\gamma a_j \widehat{p}/\hbar]^m}{m!},$$

then

$$|\Psi\rangle = \sum\nolimits_J c_j'^* c_j \left\{ 1 - \frac{i}{\hbar}\gamma A_w \widehat{p} + \sum_{m=2}^{\infty} \frac{[-i\gamma \widehat{p}/\hbar]^m}{m!} \left(A^m\right)_w \right\} |\phi\rangle \approx \left\{ \sum\nolimits_J c_j'^* c_j \right\} e^{-\frac{i}{\hbar}\gamma A_w \widehat{p}} |\phi\rangle$$

in which case

$$|\Psi\rangle \approx \langle \psi_f | \psi_i \rangle \widehat{S}(\gamma A_w) |\phi\rangle \tag{4}$$

so that

$$|\langle q| \Psi\rangle|^2 \approx |\langle \psi_f | \psi_i \rangle|^2 \left| \langle q| \widehat{S}(\gamma \operatorname{Re} A_w) |\phi\rangle \right|^2$$

or

$$|\Psi(q)|^2 \approx |\langle \psi_f | \psi_i \rangle|^2 |\phi(q - \gamma \operatorname{Re} A_w)|^2 . \tag{5}$$

Here

$$\left(A^m\right)_w = \frac{\sum_J c_j'^* c_j a_j^m}{\sum_J c_j'^* c_j} = \frac{\langle \psi_f | \widehat{A}^m | \psi_i \rangle}{\langle \psi_f | \psi_i \rangle},$$

with the *weak value* A_w of $\widehat{A}$ defined by

$$A_w \equiv \left(A^1\right)_w = \frac{\langle \psi_f | \widehat{A} | \psi_i \rangle}{\langle \psi_f | \psi_i \rangle}. \tag{6}$$

From this expression it is obvious that A_w is - in general - a complex valued quantity that can be calculated directly from theory. Since $\phi(q)$ is real valued, then eq.(5) corresponds to a broad pointer position distribution with a single peak at $\langle q \rangle = \gamma \operatorname{Re} A_w$ with $\operatorname{Re} A_w$ as the measured value of $\widehat{A}$. This condition occurs when both of the following inequalities relating γ and the pointer momentum uncertainty Δp are satisfied [7, 10] :

$$\Delta p \ll \frac{\hbar}{\gamma} |A_w|^{-1} \text{ and } \Delta p \ll \min_{(m=2,3,\cdots)} \frac{\hbar}{\gamma} \left| \frac{A_w}{(A^m)_w} \right|^{\frac{1}{m-1}}. \tag{7}$$

It is important to keep in mind that although the weak measurement of $\widehat{A}$ occurs at time t_0 so that $|\psi_i\rangle$ and $|\psi_f\rangle$ are states at t_0, these states result from states that are pre-selected and post-selected at times $t_i < t_0$ and $t_f > t_0$, respectively. Therefore it is necessary to propagate the pre-selected state forward in time from t_i to t_0 and the post-selected state backward in time from t_f to t_0 in order to calculate A_w at t_0.

The reader is invited to consult references [4–12] for additional details concerning the theoretical and experimental aspects of weak measurements and weak values.

III. THE EXPERIMENT

A. Apparatus

As mentioned above, the setup for this experiment follows that of the optical *gedanken* experiment discussed in [4] where a twin Mach-Zehnder interferometer is used to replicate aspects of the two-slit interference experiment. A schematic of the apparatus used in this experiment is shown in figure 1. Here the paths followed by photons have been labeled using the traditional "right" (R) and "left" (L) notation $R1, R2, \cdots, R6, L2, L3, \cdots, L6$. For future reference an overlay of the "metaphorical" two slits emulated by the twin Mach-Zehnder interferometer is also provided in this figure. Note that paths $R4$ and $L4$ correspond to photon paths through the right and left slits, respectively. Thus, blocking path $L4$ corresponds to closing the left slit.

Since photons do not interact with one another, it is not necessary to perform the experiment in such a manner that only one photon at a time traverses the interferometer. Accordingly, large ensembles of photons of wavelength 637.2 nm produced by a classically intense laser diode source were used in this experiment. A 150 μm diameter pinhole spa-

tially filtered the photon beam into a smooth Gaussian-like shape. The exiting beam had an optical power of 24.5 μW ($\sim 7.9 \times 10^{13}$ photons/s) and was collimated with a 200 mm focal length lens. A mirror launched the collimated beam into the interferometer via the input path $R1$. Three identical non-polarizing cube 50/50 beam-splitters - labeled BS1, BS2, BS3 in figure 1 - along with four identical mirrors - labeled M1, M2, M3, M4 in figure 1 - formed the basic architecture of the interferometer (the collection BS1, M1, M2, and BS2 (BS2, M3, M4, and BS3) is hereafter referred to as "*the first (second) Mach-Zehnder*"). The beam emerging along path $R6$ was neutral density filtered before reaching a 640×480 pixel resolution machine vision camera which recorded the beam's two dimensional intensity distribution. The optical power of the beam reaching the camera was approximately four to five orders of magnitude smaller than that exiting the pinhole. Each camera pixel had a size $7.4\ \mu m \times 7.4\ \mu m$ and a $0 - 255$ digital intensity range. The pixel saturation level exceeded the measured maximum pixel intensity level of the images obtained from this experiment.

The *gedanken* experiment utilized slightly tilted thin glass plates placed at locations in paths $R2$ and $L2$ to perform weak measurements of the projection operators $|R2\rangle\langle R2|$ and $|L2\rangle\langle L2|$ by producing transverse spatial shifts in the photon paths that were small relative to the uncertainty in the transverse position of a photon. The theoretically predicted change in the weak values of these operators when path $L4$ is blocked was interpreted as an observable effect induced in the first Mach-Zehnder by an associated non-local exchange of modular momentum produced by blocking path $L4$ in the second Mach-Zehnder (direct measurement of the modular momentum exchange is not possible because blocking path $L4$ in the second Mach-Zehnder makes the modular variable completely uncertain - thereby destroying all information about the modular momentum).

In this experiment, however, a piezoelectrically driven computer controlled stage was used instead to produce small changes in the location of mirror M1 (in the direction shown in figure 1) in order to produce a series of transverse spatial shifts in the photon beam that could be made small compared to the uncertainty in a photon's transverse position. This approach proved more efficient than the tilted plate method and was equivalent to performing weak measurements of the projection operator $|L2\rangle\langle L2|$ located in path $L2$. As shown - both theoretically and experimentally - below, the weak value of $|L2\rangle\langle L2|$ changes in accordance with the *gedanken* experiment when path $L4$ is blocked. This change can also be interpreted as a dynamical non-locality induced effect.

By avoiding the use of micro-positioners as much as possible, the setup was passively stable for several tens of minutes. The entire apparatus was also enclosed in a $1\ m \times 1\ m$ covered box to provide additional isolation from the environment. In order that the box not have to be uncovered during a measurement data run, electromagnetic shutters were used as much as possible to block and unblock photon paths and the piezoelectric stage and camera were computer controlled using data collected by the camera. Because of these features, all required measurement data were collected before opto-mechanical instability occurred using only one initial fine alignment. A data analysis and graphing software tool was developed and used to automatically process the camera images.

B. Overview

The essence of this experiment involved comparing the measured weak values of the operator $|L2\rangle \langle L2| \equiv \widehat{N}$ for two distinct (data) classes of weak measurements. For each of these weak measurement classes the pre-selected state prior to the time of $\widehat{N}$'s measurement was the spatial mode $|R1\rangle$ and the post-selected state after $\widehat{N}$'s measurement time was the spatial mode $|R6\rangle$. Also, for each of these classes the path lengths in the first Mach-Zehnder were arranged so that photons effectively only emerged from BS2 along path $R4$ in spatial mode $-|R4\rangle$. Thus, paths $R4$ and $L4$ will be referred to as the "bright" and "dark" paths, respectively. Arranging the first Mach-Zehnder in this way corresponded to localizing a photon at the right slit of a two slit screen prior to its traversing the screen. Weak measurements of $\widehat{N}$ for both measurement classes were made while the apparatus was in this configuration - except that a shutter blocked path $L4$ for the second measurement class. Blocking path $L4$ in this manner corresponded to closing the left slit in a two slit screen while the photon is localized at the right slit.

If $N_{w,1}$ and $N_{w,2}$ correspond to the weak values of $\widehat{N}$ for the first and second measurement classes, respectively, then - since $L4$ is a dark path - it might be expected that blocking path $L4$ should have no effect upon the weak measurement of $\widehat{N}$ in $L2$, in which case $N_{w,1} = N_{w,2}$. However, when eq.(6) is used to calculate these weak values it is found that for the first measurement class (which corresponds to both slits being open) $N_{w,1} = +1$ and for the second measurement class (which corresponds to closing the left slit) $N_{w,2} = +\frac{1}{2}$. More specifically, for the first measurement class, forward propagation of the pre-selected state

$|R1\rangle$ and backward propagation of the post-selected state $|R6\rangle$ through the interferometer to where $\widehat{N}$ is measured yields the states $\frac{1}{\sqrt{2}}\left(i\,|L2\rangle + |R2\rangle\right)$ and $i\,|L2\rangle$, respectively, so that

$$N_{w,1} = \frac{\left[-i\,\langle L2|\right]\widehat{N}\left[\frac{1}{\sqrt{2}}\left(i\,|L2\rangle + |R2\rangle\right)\right]}{\left[-i\,\langle L2|\right]\left[\frac{1}{\sqrt{2}}\left(i\,|L2\rangle + |R2\rangle\right)\right]} = +1$$

(note that the theoretical weak value of $|R2\rangle\langle R2|$ is 0). Similarly, for the second measurement class - with the dark path $L4$ blocked - forward propagation of the pre-selected state $|R1\rangle$ and backward propagation of the post-selected state $|R6\rangle$ through the interferometer to where $\widehat{N}$ is measured yields the states $\frac{1}{\sqrt{2}}\left(i\,|L2\rangle + |R2\rangle\right)$ and $\frac{1}{2}\left(i\,|L2\rangle + |R2\rangle\right)$, respectively, so that

$$N_{w,2} = \frac{\left[\frac{1}{2}\left(-i\,\langle L2| + \langle R2|\right)\right]\widehat{N}\left[\frac{1}{\sqrt{2}}\left(i\,|L2\rangle + |R2\rangle\right)\right]}{\left[\frac{1}{2}\left(-i\,\langle L2| + \langle R2|\right)\right]\left[\frac{1}{\sqrt{2}}\left(i\,|L2\rangle + |R2\rangle\right)\right]} = +\frac{1}{2}$$

(note that the theoretical weak value of $|R2\rangle\langle R2|$ is also $+\frac{1}{2}$).

Thus, $N_{w,1} \neq N_{w,2}$ so that - similar to the *gedanken* experiment - weak value theory applied to this experiment predicts that blocking path $L4$ produces a dramatic observable change in the weak value of $\widehat{N}$ when there are effectively no photons along path $L4$. Following [4] and using the two-slit case along with eq.(2) as guides, $N_{w,1} \neq N_{w,2}$ *has an interpretation as being an effect induced in the first Mach-Zehnder by the non-local exchange of modular momentum that results from a change in the potential associated with blocking the dark* $L4$ *path in the second Mach-Zehnder.*

A third class of weak measurements of $\widehat{N}$ designated by the weak value $N_{w,0}$ was used for the purpose of order compliance. For this measurement class the configuration of the first Mach-Zehnder was the same as for the other two classes so that forward propagation of the pre-selected state $|R1\rangle$ through the first Mach-Zehnder yielded the state $-\,|R4\rangle$. Here, however, a relative (to the other two classes) phase shift of π *rad* was introduced into path $R5$ so that backward propagation of the post-selected state $|R6\rangle$ backwards through the interferometer gives $|R2\rangle$ as the state where the measurement is made. Again using $\frac{1}{\sqrt{2}}\left(i\,|L2\rangle + |R2\rangle\right)$ as the forward propagated pre-selected state yields the weak value

$$N_{w,0} = \frac{\left[\langle R2|\right]\widehat{N}\left[\frac{1}{\sqrt{2}}\left(i\,|L2\rangle + |R2\rangle\right)\right]}{\left[\langle R2|\right]\left[\frac{1}{\sqrt{2}}\left(i\,|L2\rangle + |R2\rangle\right)\right]} = 0$$

(note that the theoretical weak value of $|R2\rangle\langle R2|$ is $+1$). This class of measurements served as a data consistency check by demonstrating that the weak values $N_{w,0}$, $N_{w,1}$, and $N_{w,2}$

measured by this experiment were compliant with the theoretical ordering requirement

$$N_{w,0} < N_{w,2} < N_{w,1}. \tag{8}$$

IV. RESULTS

In order to experimentally demonstrate this induced $N_{w,1} \neq N_{w,2}$ effect, three sequences of weak measurements of $\widehat{N}$ - one sequence for each of the $N_{w,0}$, $N_{w,1}$, and $N_{w,2}$ measurement classes - were generated following the configuration prescriptions outlined in the above overview of the experiment. Different interaction strength (γ) values were produced for each sequence by varying the M1 position via controlling that of the piezoelectric stage. The photon beam intensity served as the measurement pointer for the apparatus and its image was recorded by the machine vision camera for each M1 position used in the measurement sequences. As indicated on figure 1, the associated movement of the pointer in the image plane was horizontal (i.e. in the plane of the apparatus). For each M1 position x, the analysis software tool used the associated pointer image to locate the pointer position as the intensity averaged horizontal pixel number $\overline{y}$. Each such measurement was represented as the pair $(x, \overline{y})$. Let S_i be the set of such measurement pairs for the $N_{w,i}$ measurement class, $i = 0, 1, 2$.

To calibrate the experimental data, a fourth sequence of measurements was made to relate M1 positions to pointer pixel positions. Here, paths $L3$ and $R4$ were blocked by shutters and a sequence of M1 positions were used to sweep the beam emerging along path $R6$ across the image plane of the camera. As was the case for the previous sequences of measurements, the beam's intensity averaged horizontal pixel number was determined from each M1 position image and represented as an ordered pair $(x, \overline{y})$. Let S_3 be the set of these ordered pairs of calibration measurements.

Fourteen M1 positions equally spaced over a 1300 μm range were used to generate fourteen ordered pairs of measurements in each set S_k, $k \in K \equiv \{0, 1, 2, 3\}$. These M1 positions were identical for each of the four measurement sequences (i.e. for every $(x, \overline{y}) \in S_k$, $k \in K$, there is exactly one $(x', \overline{y}') \in S_j$, $j \in K - \{k\}$, such that $x = x'$). Examination of the measurement pairs in S_1 and S_2 revealed the existence of a data crossing point located between the middle two M1 positions x_7 and x_8. The pair (x_0, y_0) defined by the intersection of the line containing the middle two measurement pairs in S_1 with that containing the middle two measurement

pairs in S_2 was selected as the estimate of this crossing point.

Recall from eq.(5) that in the weak measurement regime defined by inequalities (7) the ordinates in each data pair in the sets S_i effectively record the measured quantity $\gamma N_{w,i}$, $i = 0, 1, 2$. Thus, at the crossing point the condition $\gamma N_{w,1} = \gamma N_{w,2}$ must hold true. Since $N_{w,1} = +1$ and $N_{w,2} = +\frac{1}{2}$, this condition can only be satisfied if $\gamma = 0$. This identified (x_0, y_0) as the point where the interaction strength γ vanishes and defined it as the origin of the Cartesian reference frame $\mathcal{F}$ which has as its abscissa axis M1 displacements in μm referenced to x_0 and as its ordinate axis pointer pixel displacements referenced to y_0. Let $(x', \overline{y}') \in S_k'$ be $(x, \overline{y}) \in S_k$, $k \in \{0, 1, 2\}$, transformed into $\mathcal{F}$ according to $x' = x - x_0$ and $\overline{y}' = \overline{y} - y_0$.

As anticipated - the calibration measurement pairs in S_3 were linear. The associated slope which relates pointer pixel positions to M1 positions in μm was -0.198. This slope defined the calibration line $\overline{y}' = -0.198x'$ in $\mathcal{F}$. Multiplying the slope of this equation by the pixel size 7.4 μm (the camera rated distance between consecutive pixels) yielded the equation $\gamma(x') = -1.5x'$ in which both γ and x' are in μm. The ordinate $\overline{y}'$ is relabeled as $\gamma(x')$ in this equation because it now directly relates the interaction strengths of measurements to the displacement of M1 (inspection of the argument of the operator $\widehat{S}$ in eq.(4) reveals that γ is a distance since $N_{w,i}$ is a dimensionless quantity). Thus - for this experiment - the "ideal" pointer displacements $\rho_i(x') \equiv \gamma(x') N_{w,i}$ in μm as functions of M1 displacements in μm and $N_{w,i}$ values are represented by the lines

$$\rho_i(x') = -1.5x' N_{w,i},\ i = 0, 1, 2. \tag{9}$$

This result is useful for estimating the boundaries of the weak measurement regime for this experiment in terms of x'. Since $\widehat{N}$ is a projection operator then $\widehat{N}^m = \widehat{N}$, $m \geq 1$, so that $(N^m)_{w,i} = N_{w,i}$ and inequalities (7) become $\Delta p \ll \frac{\hbar}{\gamma N_{w,i}}$, $i \neq 0$, and $\Delta p \ll \frac{\hbar}{\gamma}$. Application of the uncertainty relation $\Delta q \cdot \Delta p \geq \frac{\hbar}{2}$ yields $\gamma \ll \frac{2\Delta q}{N_{w,i}}$, $i \neq 0$, and $\gamma \ll 2\Delta q$. Both of these inequalities are satisfied by $\gamma \ll 2\Delta q$ when $i = 1, 2$. Using the pinhole diameter as the uncertainty in a photon's tranverse position, i.e. $\Delta q \approx 150\ \mu m$, defines $|\gamma| \ll 300\ \mu m$ as the estimated weak measurement regime for the interaction strength ($|\gamma|$ is used since in this experiment γ can be a positive or a negative distance). Using this range in eq.(9) with $N_{w,1} = +1$ gives $\rho_1(x') = \gamma(x')$ and yields

$$|x'| \ll 200\ \mu m \tag{10}$$

as the estimated weak measurement regime for M1 displacement.

A plot of the measurement pairs in sets S_i', $i = 0, 1, 2$ is presented in figure 2. Here the ordinate of each measurement pair has been scaled by the pixel distance of 7.4 μm in order to express the pointer displacements in μm. Also shown as dashed lines are graphs of the three ideal pointer displacement lines $\rho_i(x')$, $i = 0, 1, 2$, given by eq.(9) and as a boxed region the estimated weak measurement regime defined by inequality (10). Inspection of figure 2 (where $\gamma N_{w,i}$ data points are labeled "γN class i" and ρ_i is labeled "ρ class i") reveals good agreement within (and slightly outside) the weak measurement regime between the measured pointer displacements $\gamma N_{w,1}$ (corresponding to the measurement pairs in set S_1') and ρ_1 and between the measured pointer displacements $\gamma N_{w,2}$ (corresponding to the measurement pairs in set S_2') and ρ_2. It is also clear that - except at x_8' - the measured quantities within the weak measurement regime are compliant with the theoretical ordering requirement (8). It is noted that the $\sim 75\ \mu m - 100\ \mu m$ offsets of the measured pointer displacements $\gamma N_{w,0}$ (corresponding to the measurement pairs in set S_0') from ρ_0 in the weak measurement regime are likely due to complicated intensity profile inversions introduced by the phase window during this sequence of measurements. Interestingly, if these offsets are treated as a constant bias, then removal of the bias from the measurement pairs in S_0' not only produces complete compliance with (8) in the weak measurement regime - but it also provides more overall symmetry in the data, as well as good agreement between the measured pointer displacements $\gamma N_{w,0}$ and ρ_0 in the weak measurement regime.

As expected, the further the M1 displacement is outside the weak measurement regime the "stronger" the measurement becomes and the greater the discrepancy between the S_0' data and ρ_0 and between the S_1' data and ρ_1. However, except for the data asymmetry associated with negative M1 displacements (likely introduced by the complicated optical properties of the apparatus), the agreement between the S_2' data and ρ_2 remains good over the entire range of M1 displacements while the S_0' and S_1' data converge to ρ_2. This feature in the data is completely consistent with the fact that in the limit of "strong collapsing" measurements, the measurement pointer is displaced by $\gamma \langle N \rangle = \frac{1}{2}\gamma$ since

$$\langle N \rangle = \frac{1}{\sqrt{2}} \left[-i \langle L2| + \langle R2| \right] \widehat{N} \left[i |L2\rangle + |R2\rangle \right] \frac{1}{\sqrt{2}} = +\frac{1}{2}$$

(refer to the discussion surrounding eq.(3)).

V. CONCLUDING REMARKS

This experiment used weak measurements of pre- and post-selected ensembles of photons in a twin Mach-Zehnder interferometer to observe an effect theoretically predicted to be induced in the first Mach-Zehnder by the non-local exchange of modular momentum produced by blocking the dark path in the second Mach-Zehnder (it is intended that a second "follow up" paper be written which will detail the novel aspects of the apparatus and techniques used in this experiment). This effect is manifested as a dramatic change in the associated weak values. The attendant weak values measured by this experiment changed in complete accordance with the theoretical predictions. Consequently, the results of this experiment support both the existence of such an effect and the authenticity of dynamical non-locality as its cause.

Before closing, it is noted that - although this experiment was specifically designed for the purpose of confirming or denying the $N_{w,1} \neq N_{w,2}$ effect - it was observed that - for the weakest measurements with abscissa $x_8 \simeq 37\ \mu m$ - the ratio of the number of camera pixels excited by the associated S_2' measurement to that excited by the associated S_1' measurement was 0.6. The drop in this excitation ratio was 4 to 5 times greater than expected based upon the alignment contrast ratios for the apparatus. This informal observation provides additional credence to dynamical non-locality as inducing the $N_{w,1} \neq N_{w,2}$ effect and suggests a future experiment that could further examine dynamical non-locality from this perspective.

Acknowledgments

The authors thank Yakir Aharonov and Jeff Tollaksen for suggesting this experiment; John Gray and James Troupe for constructive technical discussions; and David Niemi for his efforts in the instrumentation of this experiment. Special thanks are given to Susan Hudson, Electromagnetic and Sensor Systems Department Head, for her commitment to this research. This work was supported in part by a grant from the NSWCDD ILIR program sponsored by the Office of Naval Research.

---

[1] Tonomura A, Endo J, Matsuda T, Kawasaki T and Ezawa H 1989 *Am. J. Phys.* **57** 117

[2] Aharonov Y, Pendelton H and Peterson A 1969 *Int. J. Theor. Phys.* **3** 213

[3] Aharonov Y, Pendelton H and Peterson A 1970 *Int. J. Theor. Phys.* **3** 443

[4] Tollaksen J, Aharonov Y, Casher A, Kaufherr T and Nussinov S 2010 *New J. Phys.* **12** 013023

[5] Aharonov Y and Rohrlich D 2005 *Quantum Paradoxes: Quantum Theory for the Perplexed* (Weinheim : Wiley-VCH) p 67, p 225

[6] Aharonov Y, Albert D and Vaidman L 1988 *Phys. Rev. Lett.* **60** 1351

[7] Duck I, Stevenson P and Sudarshan E 1989 *Phys. Rev. D* **40** 2112

[8] Aharonov Y and Vaidman L 1990 *Phys. Rev. A* **41** 11

[9] Ritchie N, Story J and Hulet R 1991 *Phys. Rev. Lett.* **66** 1107

[10] Parks A, Cullin D and Stoudt D 1998 *Proc. Roy. Soc. Lond. A* **454** 2997

[11] Hosten O and Kwiat P 2008 *Science* **319** 787

[12] Dixon P, Starling D, Jordan A and Howell J 2009 *Phys. Rev. Lett* **102** 173601

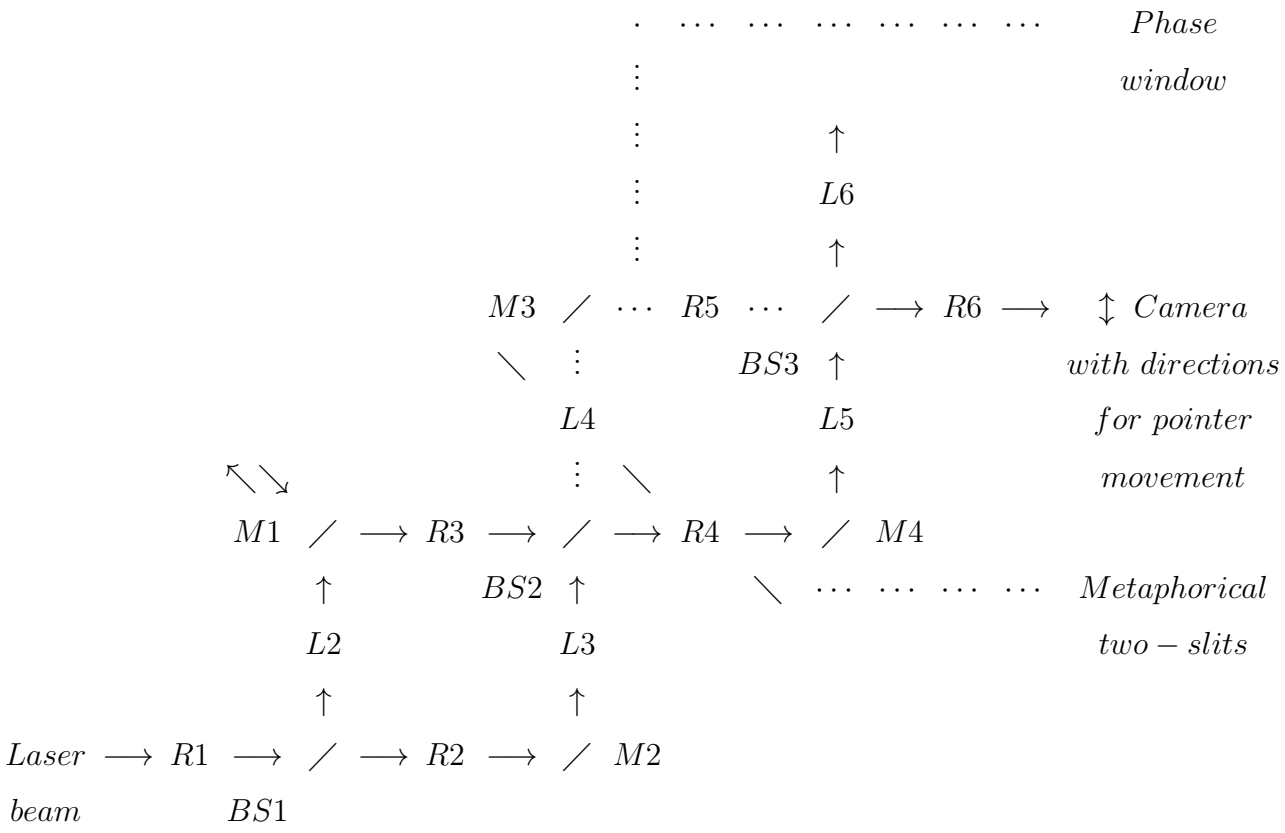

(Figure 1. Apparatus, best available diagram for electronic publishing)

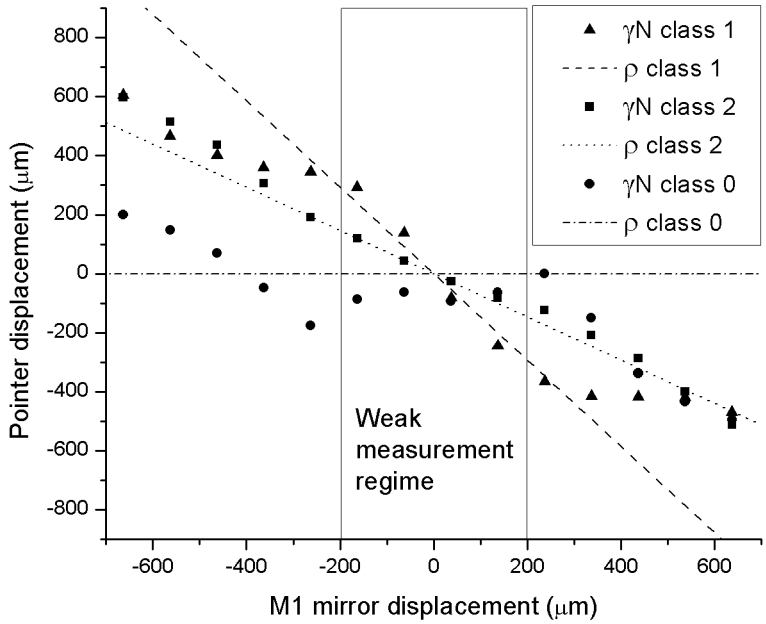

Figure 2. Experimental data